A quantitative and qualitative analysis of Positron Emission Tomography (PET) in Yttrium-90 radioembolization; investigating the utility of PET dosimetry in identifying sites of necrosis and viable tumor

Yasaman Anbari Yazdi

Student number:
2102865

Supervisors:

Prof. Dr. Marnix Lam

Clin. Sci. Grace Keane

Department of Radiology and Nuclear Medicine, University Medical Center Utrecht, Utrecht, The Netherlands

Faculty of Medicine, University of Turku, Finland

Abstract

Purpose: PET imaging is becoming more common for verifying the location of ^{90}Y microspheres during liver cancer treatment. The work aims to predict which patients will likely to have remaining viable tumors based on the ^{90}Y PET image taken right after the radioembolization.

Methods: 10 hepatocellular carcinoma (HCC) patients treated by radioembolization with ^{90}Y glass microspheres were included in this study. Post-treatment PET was coregistered with the follow-up image to investigate the correlation between the isodose contours based on the post-treatment PET image and the necrosis and viable tumor on the follow-up image. To evaluate the similarity quantitatively, isodose contours derived from ^{90}Y PET and necrosis area on the follow-up image were compared using the Dice similarity coefficient. In addition to the quantitative assessment, a qualitative assessment of a 1–5-point scale was utilized to rate the correlation of underdose regions on the post-treatment PET and the viable tumor on the follow-up. The study thereby provided insights into the interpretation and analysis of post-radioembolization imaging in HCC patients.

Results: The findings in this retrospective study with 10 patients included for quantitative assessment suggest an isodose range of 250 Gy to 300 Gy yields the best match for the necrosis site. Also, the qualitative assessment of these 10 patients shows a median agreement of 4 on a 1–5-point scale.

Conclusion: ^{90}Y PET/CT evaluation and dosimetry add clinical benefit to patient treatments by locating untreated tumors and potential sites of recurrence.

Keywords: yttrium-90 microspheres, primary liver cancer, selective internal radiation therapy, trans-arterial radioembolization, post-treatment dosimetry

List of Abbreviations

^{18F}FDGPET	Fluorine-18 fluorodeoxyglucose positron emission tomography
^{90}Y	Yttrium-90
BCLC	Barcelona clinic for liver cancer
BSA	Body surface area
CR	Complete response
CT	Computerized tomography
DoR	Duration of response
ESMO	European Society of Medical Oncology
GI	Gastro-intestinal
HCC	Hepatocellular carcinoma
LFS	Lung shunt fraction
mCRC	Metastatic colorectal cancer
MIRD	Medical internal radiation dose
mRECIST	Metastatic colorectal cancer
MRI	Magnetic Resonance Imaging
ORR	Overall response rate
OS	Overall survival
PD	Progressive disease
PET	Positron emission tomography
PFS	Progression-free survival
PR	Partial response
RECIST	Response Evaluation Criteria in Solid Tumors
REILD	Radioembolization-induced liver disease

SD	Stable disease
SIRT	Selective internal radiation therapy
SPECT	Single-photon emission computerized tomography
T/N	Tumor-to-normal uptake ratio
TACE	Transcatheter arterial chemoembolization
TARE	Transarterial radioembolization
TTP	Time to progression
$^{99\,m}$Tc-MAA	Technetium-99m macroaggregated albumin

Table of Contents

1. Introduction

1.1. Preface

Radioembolization with yttrium-90 (^{90}Y) microspheres allows for highly targeted delivery of internal radiation to liver tumors, making the therapy promising for unresectable hepatocellular carcinoma (HCC). However, the determinants of treatment response remain unclear in some patients. Notably, some patients demonstrate viable tumors on the follow-up despite receiving tumoricidal radiation doses exceeding the recommended dose for the whole tumor. This raises a critical question: Why do some patients have residual viable tumors even after high-dose radioembolization?
The present thesis addresses this question through dosimetric analysis of ^{90}Y PET imaging to evaluate intratumoral dose distribution. We hypothesize that intra-tumoral dose heterogeneity, resulting in sub-therapeutic dosing of portions of the tumor, explains these findings. By characterizing dose metrics within tumor sub-regions like isodose contours. If we identify that an isodose range corresponds well with the viable tumor we see on the follow-up image, we can predict the presence of a residual tumor based on the PET scan after treatment. The findings of this thesis demonstrate the importance of patient-specific intratumoral dosimetry in radioembolization to identify areas of potential undertreatment, which could have important implications for patient care.

1.2. Background

Hepatocellular carcinoma

HCC is the most prevalent form of liver cancer among primary liver malignancies, which targets hepatocytes, the main type of liver cells. HCC causes half a million deaths every year worldwide. It is the fifth most commonly diagnosed cancer and the leading cause of cancer-related deaths worldwide.
For choosing the proper treatment for HCC, it is essential to consider the disease stage. Therefore, the Barcelona Clinic Liver Cancer (BCLC) staging system was developed to categorize HCC into 5 stages (0/A/B/C/D) according to tumor burden, liver function, and the Child–Pugh classification system. Besides providing a prognosis for HCC, this staging system offers therapeutic strategies for each state.
According to the latest BCLC algorithm (Fig.1), among HCC patients who are not candidates for curative liver resection or liver transplantation, locoregional treatment

plays an important role in reducing tumor burden, relieving symptoms, and increasing survival. For this purpose, various agents, including chemotherapy agents, embolic particles, and radioactive materials, are currently injected into tumors through feeding vessels to achieve cytoreduction by allowing more focused delivery or deposition of higher concentrations within the tumor.

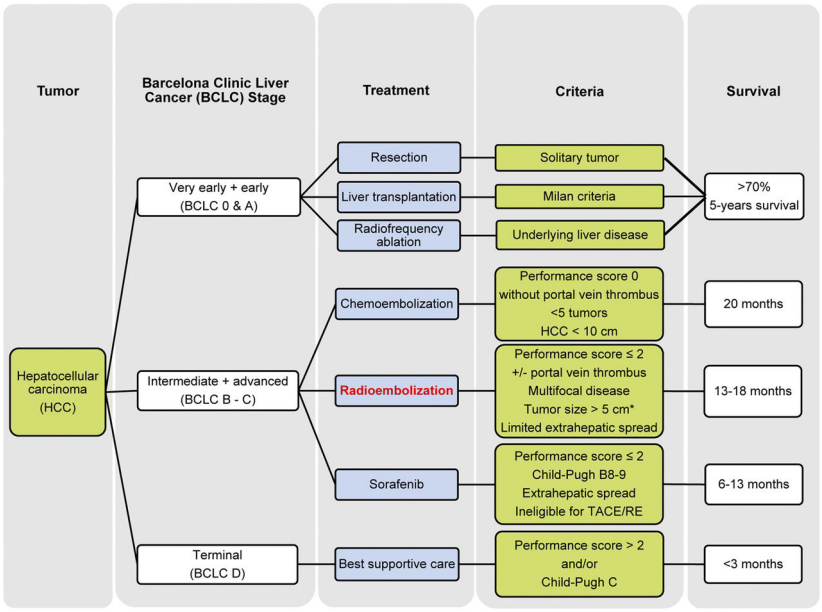

Fig.1 BCLC staging system with the proposal for radioembolization in the treatment paradigm[1]. This figure is reprinted with the copyright holder's permission.

Radioembolization

Radioembolization is one of the treatment options for intermediate and advanced HCC patients. It is a minimally invasive procedure that combines radiation and embolization to achieve two goals simultaneously. The first is to deliver a high radiation dose to the tumor, which helps destroy cancer cells while minimizing the radiation exposure of healthy surrounding tissue. The second is to block the blood supply to the tumor. Upon injection of microspheres into the hepatic artery, they become lodged in the blood vessels that supply the tumor with blood, cause blockage, and reduce blood supply, causing tumor shrinkage.

Liver vascularization

This novel treatment is based on the liver's unique dual vascularization. Research on the blood supply to the liver reveals that tumors in the liver derive 80%–100% of their blood supply from the arterial circulation. In contrast, the liver parenchyma receives blood from the portal vein. Through the intra-arterial administration of microspheres

embedded in a beta-emitting isotope, yttrium-90, a high radiation dose is delivered to the solid tumor to minimize the dose to the healthy liver parenchyma.[2]

Microspheres

Currently, two different kinds of yttrium-90 microspheres are commercially available: ^{90}Y glass microspheres (TheraSphere®, Boston Scientific) and resin ^{90}Y microspheres (SIR-Spheres®, Sirtex Medical Ltd.). Both products are CE-marked (affirmed European health standards) to treat unresectable liver tumors in Europe. However, in the USA, TheraSphere was FDA-approved for treating HCC, SIR-Spheres was under a humanitarian device exception, and resin microspheres are approved for treating metastatic colorectal cancer (mCRC) when combined with adjuvant therapy and floxuridine.[3]

Both ^{90}Y emit β-radiation with a comparable energy level and therapeutic mechanism. The primary difference between glass and resin microspheres is the higher activity of individual glass particles, which allows for fewer microspheres with high activity to be used in treatment. Additionally, glass microspheres result in a lower dose absorbed by healthy liver tissue, while a higher dose absorbed by liver lesions reduces the incidence of ectopic embolism caused by reflux.[4] On the other hand, resin microspheres have a lighter specific gravity than glass microspheres, which are closer to blood, resulting in a more even distribution within tumors. Furthermore, resin microspheres are well-spheroidized and quickly prepared for injection. The administration of either glass or resin microspheres is based on the principle that liver lesions are almost solely supplied by the arterial stream, while normal liver parenchyma is mainly supplied by the portal vein. ^{90}Y microspheres embolize in the peripheral blood vessels of the tumor and accumulate in its microvasculature because they cannot pass through the capillary bed of the tumor. The distribution of the radioactive ^{90}Y in the arterioles and capillaries in and around the tumors results in the emission of high-energy beta-radiation in the liver lesions, inducing cell death while sparing the healthy liver parenchyma. The local ionizing radiation dose is as high as 100–150 Gy, causing severe DNA damage in tumor cells and producing a solid tumoricidal effect. Since the tissue penetration of ^{90}Y in the liver is only 2.5 mm, ^{90}Y causes minor damage to normal tissue. Unlike traditional transcatheter arterial chemoembolization (TACE), ^{90}Y radioembolization therapy mainly depends on the radiation effect of ^{90}Y microspheres, playing an anti-tumor role, rather than the hypoxia caused by embolism or the chemotherapeutic effect of drugs.

^{90}Y MICROSHPERE CHARACTERISTICS		
RADIOISOTOPE CHARACTERISTICS	Half-life: 64.2 hours Approximated deposited energy per activity: 49,67 J/GBq Maximum tissue penetration: 2.5-1 mm Imaging possibilities: PET (internal pair production) and SPECT (Brehmsstralung)	
MANUFACTURER	**SIR-Spheres, Sirtex Medical**	**TheraSphere, Boston Scientific**
CARRIER	Resin microspheres	Glass microspheres
SPECIFIC ACTIVITY	50-200 Bq	250-2500 Bq
SIZE RANGE	20-60 µm	20-30 µm
EMBOLIZING EFFECT	Moderate	Low
APPROVAL CE AND FDA	CE and FDA	CE and FDA
DENSITY	1.6 g/mL (comparable to red blood cells)	3.3 g/mL
MAXIMUM BETA ENERGY	2.28 MeV	2.28 MeV
MICROSPHERES PER VIAL	44 (±2.6) million	Variable

Table. 1 Comparing resin and glass microspheres

Delivery approach

The process of radioembolization involves microspheres containing radioisotopes, implanted into the liver through various methods: a whole-liver, lobar, or selective/segmental approach. Fig.2 shows the following: A) While a whole-liver approach in a single session is not commonly performed, current practice often involves a staged procedure that treats the dominantly diseased lobe first. Lobar radioembolization is frequently used to address multiple lesions within a specific liver lobe. B) Radiation lobectomy (RL) is an approach characterized by delivering a subablative dose to the entire lobe. It has been used as a definitive treatment option for large, unresectable hepatic tumors or as a surgical neoadjuvant. RL is effective in achieving disease control and hypertrophy of the contralateral lobe by delivering a high radiation dose to both tumors and normal liver parenchyma (>70 Gy).[5] C)) A third option is radiation segmentectomy (RS), which involves selectively perfusing 9 portal Couinaud–Bismuth segments with radioisotopes to deliver an ablative dose to individual segments of the liver. RS is used as a definitive treatment option for unsuitable surgical candidates. Additionally, it permits repeat transarterial treatment.[6]

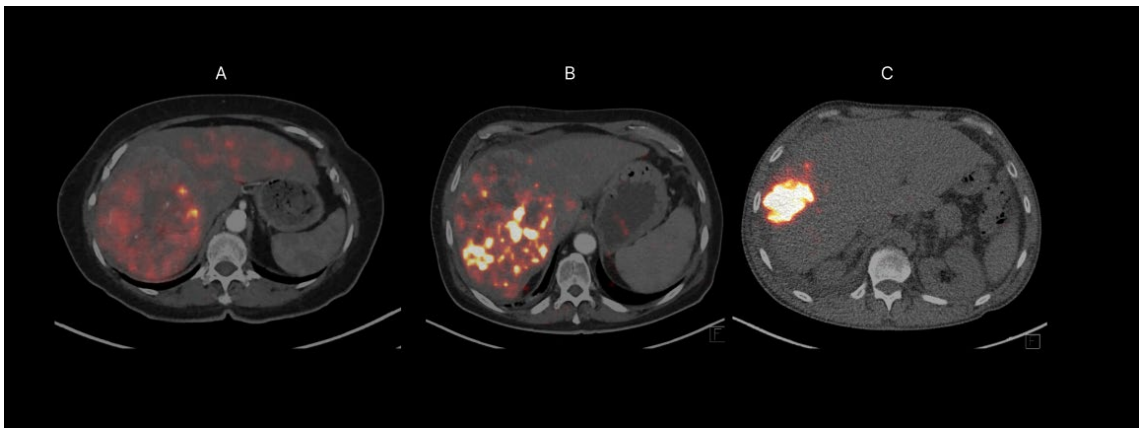

Fig.2 Fig.2 Examples of different delivery approaches: Depending on the anatomic distribution of the tumors, concomitant factors affecting liver function, and institutional preferences, a delivery method can be selected. A) A whole-liver delivery approach is advantageous in treating many tumors with good coverage of tumor vascular beds. B) The lobar treatment approach—the delivery of microspheres to the right lobe—is widely used in multifocal and advanced-stage diseases for palliation. C) The segmental approach—the infusion of an ablative dose of microspheres to one or two liver segments—is usually used for an early-stage disease as a definitive treatment.

Patient eligibility for radioembolization

As stated in the most recent guideline of the European Association of Nuclear Medicine (EANM[7]), radioembolization is indicated in patients with primary and secondary liver tumors who are not candidates for surgical resection, liver transplantation, or curative ablative therapies.

Radioembolization contraindications can be divided into absolute and relative contraindications. Pregnancy and breastfeeding are absolute contraindications, as are life expectancy of fewer than three months, clinical liver failure (such as ascites, icterus, or encephalopathy), disseminated extrahepatic malignant disease (refer to the diagnostic work-up section), and cases where pretreatment intra-arterial scout dose scintigraphy (or peri-procedural C-arm CT) reveals any extrahepatic activity (gallbladder, lymph nodes, and falciform ligament are exceptions). Patients with a Child–Pugh score greater than B7 are considered relative contraindications, as these patients may develop liver decompensation after glass administration with a standard dose (i.e., single compartment modeling), particularly if the treatment is not (bi)segmental. There is also a concern regarding intrahepatic tumor burden, with the acceptable level dependent on the type of tumor. It is common to report a cut-off of 50%–70%. The acceptable level of extrahepatic tumor burden is also determined by the type of tumor. Usually, hilar lymph nodes (up to 2 cm in the short axis) and lung nodules (up to 1 cm; up to 5) are accepted.

Treatment workflow

Although HCC treatment with ^{90}Y has been shown to have several benefits in different studies, multiple factors must be considered. This complex multidisciplinary treatment needs experts from different fields, including interventional radiology, radiation oncology, nuclear medicine, medical physic, and surgical oncology, involved with ^{90}Y microsphere therapy to yield the best outcome. Several steps should be taken to ensure the best possible outcome for radioembolization

Pretreatment baseline imaging

Performing baseline diagnostic imaging, typically comprising contrast-enhanced CT or MRI, marks the first step in the radioembolization workflow. After liver tumors or metastasis is detected, patients undergo imaging to stage and evaluate the extent of the disease. Those with non-resectable and chemoresistant liver cancer are eligible for radioembolization treatment. A multidisciplinary team reviews the baseline images and liver function laboratory values to determine whether a patient is a suitable candidate for treatment.

The preparatory examination comprising angiography and scintigraphy with technetium-99m macroaggregated albumin (99mTc MAA)

Conducting a macroaggregated albumin (MAA) procedure or scout procedure prior to the radioembolization is vital in preventing toxicity associated with ^{90}Y microspheres. First, hepatic angiogram and meticulous coil embolization are performed to identify all the abdominal vessels and block the vessels that could transport the microspheres to nontarget organs such as the stomach, gallbladder, duodenum, or pancreas, respectively. Using catheter-directed CT, including C-arm cone-beam CT or hybrid angiography/CT during angiography, may permit the identification of the culprit vessels and their immediate coil embolization. C-arm CT is a useful imaging technique that combines fluoroscopy and computed tomography (CT) to produce real-time 3D images of the patient's liver anatomy. This imaging method may help the interventional radiologist to identify tumor coverage during the angiography procedure. Unenhanced tumor regions can also be detected, often leading to the identification of additional supplying arteries, preventing incomplete treatment.[8] Approximately 150 MBq ^{99m}Tc-labelled MAA is then injected into the right and left and sometimes segment IV hepatic to simulate the distribution of the therapeutic microspheres that will be formed afterward.[9]

A whole-body gamma scintigraphy scan is used to determine the distribution of ^{99m}Tc-MAA, conducted especially to assess the tracer deposition in the lungs since arteriovenous blood vessel shunts may direct microspheres to the lungs and induce potentially fatal lung toxicity. To avoid lung toxicity, a metric called lung shunt fraction (LFS) is utilized to measure the number of ^{99m}Tc-MAA particles in the lungs, which is determined by the ratio of ^{99m}Tc-MAA particle counts to the summed counts in the lungs. Single-photon emission computed tomography (SPECT) of the abdomen is acquired to indicate the tracer accumulation in nontarget organs.

Although ^{99m}Tc-MAA is currently accepted as a surrogate of the actual therapeutic ^{90}Y microspheres distribution, several studies have shown that due to differences in the morphology, density, and size of ^{99m}Tc-MAA and ^{90}Y particles, discrepancies may sometimes be observed in the distribution of ^{99m}Tc-MAA and ^{90}Y microspheres.[10] Wondergem et al. [11] reported that in every ^{99m}Tc-MAA procedure, at least one segment showed a 10% under- or overestimation. The position of the catheter tip during administrations, as well as the tumor load of the liver segments, significantly influenced the disagreement.

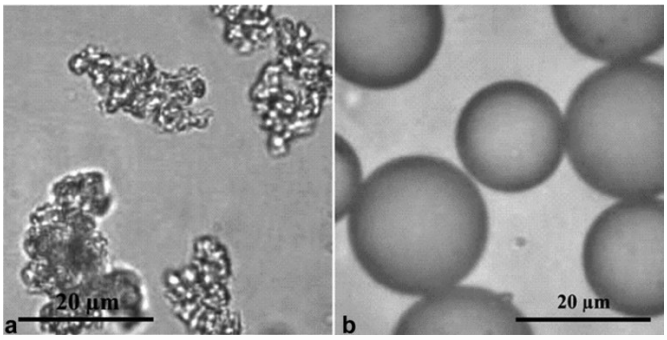

Fig.3 MAA particles (a) and TheraSphere (Boston Scientific, Marlborough, MA) microspheres (b) as viewed under a microscope: It is evident that the morphological differences between the two particles are significant (Images provided by Boston Scientific) [10]. This figure is reprinted with the permission of the copyright holder.

Treatment planning

Definitions in radioembolization dosimetry

Radioembolization is a targeted treatment for tumors with high vascular density. Microspheres containing a radiation source are used, and the effectiveness of the treatment depends on how they are deposited within the tumor's vasculature. For accurate treatment planning, it is important to differentiate between the administered radioactivity and the eventual tissue exposure. The radiation dose is measured in gray (Gy) and influenced by four factors that determine its biological impact: activity, volume, distribution, and radiation susceptibility. The activity, commonly measured in decays per second or becquerel (Bq), is typically administered in the billions for radioembolization. However, the amount of tissue in which activity is contained, variations in vascular compartments, and the radiosensitivity and repair capabilities of both tumor and normal parenchyma also play a crucial role in determining the dose and biological effects of radioembolization. Therefore, it is important to avoid oversimplifying the treatment by assuming uniform activity delivery within a target volume.[12]

Pretreatment activity measurements

The primary objective of radioembolization is to achieve the highest possible absorbed dose in tumors to maximize tumor cell apoptosis and minimize the impact on healthy tissues. Thus, successful implementation of this technique hinges on dosimetric optimization and individualized treatment planning. Pretreatment calculations for activity planning ensure an effective, safe administration of radioembolization, contributing to individualized treatment.

Over the years, numerous advances have been made in the measurement of pretreatment activity. Different methods are currently used in treatment centers, including the body surface area (BSA), the medical internal radiation dose (MIRD), and the partition.

The BSA method

BSA is the most frequently used method for calculating resin microsphere activity. This method has been explored in numerous randomized clinical trials, computing a prescribed activity based on an estimated normal liver volume derived from a patient's BSA. Despite considering tumor load, the method does not consider the absorbed doses in tissues other than tumors. Thus, the method is susceptible to underdosing and overdosing in patients with an abnormal liver size. The method may underestimate the activity required for small patients with larger livers and overestimate it for large patients with smaller livers. It should be noted that liver volume estimation data used in the method is derived from healthy individuals, which may not accurately measure the liver volume of patients with a disease. Furthermore, the method does not consider the varying intrahepatic distributions caused by differences in tumor-to-non-tumor ratios; this can result in incorrect dose distribution for patients with either hypo- or hypervascular cancerous tissues.[13]

The single-compartment MIRD method

The MIRD method, a calculation approach for a mono-compartment activity, is mainly administered for glass microspheres. The MIRD method considers the target average dose and the volume of the targeted hepatic tissue. Based on the clinical interpretation by the responsible physician, an average absorbed dose between 80 and 150 Gy can be considered for glass microspheres. The liver volumetric measurement may be achieved by CT, MRI, or PET/SPECT.

Notably, the single-compartment MIRD method assumes a homogeneous microsphere distribution within the perfused volume. In reality, the distribution of the microspheres may be heterogeneous, particularly in the case of tumors or other lesions where significant differences in uptake between different regions may exist. This heterogeneity may affect the accuracy of the absorbed dose calculations.[14]

Multi-compartment MIRD or partition method

Owing to the advances in dosimetry techniques, the most accurate and safe activity measurements have evolved. The partition model, also known as the multi-compartment method, is the most accurate and comprehensive activity planning approach used clinically today. The basis of this MIRD-derived method is the theoretical determination of the radiation activity partitioned into the tumor, non-tumorous liver, and lungs. Most of the patient-based factors overlooked by the BSA and the MIRD methods are considered in the partition method. This technique aims for the maximum absorbed dose

in the cancer tissue and the minimum absorbed dose in the lungs and the normal liver tissue.

Primary determinants of the compartmental dose and activity in the partition-based activity planning include volume (of both the liver and the tumor), shunt fraction, and T/N avidity ratio. This method usually does not consider the heterogeneous dose distribution within the compartments. However, the voxel-based multi-compartment MIRD considers the heterogeneity of the microsphere's uptake, which may be crucial for intra-tumoral dose distribution.

For the partition method, ^{99m}Tc-MAA SPECT/CT imaging is used to predict the activity within the compartments. The ^{99m}Tc-MAA is a surrogate of the actual therapeutic ^{90}Y microspheres distribution. Dissimilarities in the ^{90}Y microspheres distribution and its surrogate are a limitation of the method.

This method is a promising activity planning approach that considers patient-specific factors and aims to maximize the absorbed dose to cancerous tissue while minimizing the absorbed dose to normal tissues. However, it may be limited in its widespread use in clinical practice due to its high level of demand and accuracy limitations in volume determination and T/N ratio evaluation.[1]

Method	Activity calculation equation
Empiric[1]	≥ 50% Tumor Load = 3 GBq 25–50% tumor Load = 2.5 GBq ≤ 25% Tumor Load = 2 GBq
BSA[1]	$A(GBq) = (BSA-0.2)] + \frac{tumor\ volume}{tumor\ volume / liver\ volume}$ in which $BSA = 0.20247 \times height(m)^{0.725} \times weight(kg)^{0.425}$
MIRD[1]	$A(GBq) = [\frac{D(Gy) \times liver\ mass\ (kg))}{50 \times (1-LFS)}]$ with an upper limit of lung shunt activity: $LFS\% \times A\ (GBq) = 0.61\ GBq$
Partition[1]	$A(GBq) = [\frac{[D(Gy) \times (\left[\frac{T}{N} \times tumor\ mass(kg)\right] + liver\ mass\ (kg))}{49.670 \times (1-LFS)}]$ in which, based on MAA SPECT/CT: $T/N = \frac{Tumor\ activity\ (GBq) / tumor\ mass\ (kg)}{liver\ activity\ (GBq) / liver\ mass\ (kg)}$

Table 2. Comparing different pretreatment activity calculation equations[1]

Voxel-based dosimetry

The voxel-based dosimetry technique, which has become increasingly popular in radioembolization, provides a more precise evaluation of the intratumoral dose distribution by generating 3D voxel-based dose maps.[4] By preserving the spatial distribution of activity, this technique accurately reflects the intratumoral heterogeneity and creates absorbed dose gradients that cover the entire tumor volume. However, due to limitations in nuclear medicine imaging resolution at the voxel level, quantitative assessments of dose-volume histograms (DVHs) should be made cautiously. In an ideal situation, high-resolution image data (such as CT or MRI) would be used as the basis of the voxel dosimetry calculation.[9]

Limitations of the existing dosimetric methods

BSA and partition dosimetric methods share certain limitations, namely the nonuniform distribution of microspheres within the treated liver. It has been proven through studies that the assumption is incorrect. Microspheres are actually implanted in heterogeneous clusters at both macro- and microscopic levels, with a preference for deposition at the outer edges of the tumor.[15]

This can lead to inaccuracies in determining the actual dose distribution, especially since a microsphere's micro-distribution greatly affects where the dose is deposited. In

addition, the long beta particle range for microspheres is often neglected, leading to the "cross-fire" effect where non-targeted regions obtain a dose of radiation from neighboring targeted regions. This effect is particularly noticeable in the partition method, which has been shown to be inaccurate due to the exclusion of the cross-fire effect. Furthermore, the dose to the liver may be underestimated within the lung boundaries due to the long range of beta particles emitted from ^{90}Y. Therefore, to improve the accuracy of current clinical dosimetry methods, scientists must consider these limitations and develop new approaches that account for the complex microsphere distribution and beta particle range.

Treatment

An interventional radiologist performs this procedure by inserting a catheter into a patient's femoral artery and guiding the catheter to the correct hepatic artery using X-ray fluoroscopy. A vial containing ^{90}Y microspheres is infused into the body via the catheter. Then, dosimetry based on images taken after the 99mTcMAA procedure is used to calculate the administered activity. The dosage of ^{90}Y-TheraSphere® ranges from 1.2 to 8 million microspheres with a specific activity of 2,500 Bq per sphere. Low volumes of saline solution are typically required for the infusion, ranging from 27 to 180 ml. However, continuous fluoroscopic guidance is unnecessary as the vascular bed is not completely saturated. The complete infusion usually requires 20 to 60 ml and 5 minutes.[16] An alternate trans-radial approach has recently been deemed feasible. This method involves inserting a catheter into a patient's radial artery instead of the femoral artery. The method has advantages, such as patient preference and lower cost, albeit with more significant technical challenges.

When selecting a radioembolization treatment method, several factors must be considered, including the number and location of the tumors and the arterial perfusion. For tumors located within a single liver segment receiving blood from only one main arterial branch or main artery, performing super selective catheterization or radiation segmentectomy is recommended.[17] This is the most precise method, involving the targeting of two or fewer liver segments with a high dose of radiation, ensuring the non-tumoral tissue absorbs a reduced amount of radiation. Another treatment option is RL. This is an option when surgical resection is not feasible or when the future liver remnant is considered inadequate to support liver function. As a result of this method, tumor progression is controlled, and contralateral lobe hypertrophy is induced. Radiation-induced hepatic lobe enlargement is an intriguing consequence of radioembolization. According to Vouche et al.[5] (2013), this phenomenon happens due to radiation-induced parenchymal lesions and reduced blood supply. In this condition, portal flow is redirected toward the contralateral lobe due to radiation shrinking the irradiated lobe. Therefore, both the size and the functionality of the contralateral lobe increase. During bilateral disease treatment, sequentially infusing each lobe may help maintain the contralateral lobe's functional capacity. To proceed with the second lobe treatment, the 30-day follow-up assessment should be completed first.

Post-treatment procedure (SPECT/CT or PET/CT)

Post-treatment imaging and dosimetry

After radioembolization, post-treatment imaging with either bremsstrahlung SPECT (bSPECT) or PET scan is recommended. These scans are used to assess therapy effectiveness, calculate absorbed doses, and correlate results with clinical response. Though SPECT/CT is a widely available modality, its spatial resolution is limited, and energy window-based scatter methods cannot be used for ^{90}Y SPECT due to the absence of an identifiable energy peak in the continuous bremsstrahlung energy spectrum measured during ^{90}Y SPECT/CT.

PET/CT, on the other hand, is generally considered superior in image quality due to its higher spatial resolution. Lhommel et al. [18] first demonstrated the viability of using PET/CT for post-treatment imaging after radioembolization, yet many centers often skip this step in the workflow and proceed directly to follow-up imaging despite its importance in contemporary practice. Recent guidelines (Levillain 2021[19]) strongly advocate for post-treatment radioembolization imaging with PET, yet this step remains often neglected.

^{90}Y PET vs. bremsstrahlung SPECT

The feasibility of using ^{90}Y bremsstrahlung SPECT imaging has been investigated and approved through experimental phantom studies and clinical studies. However, due to the low photon yield and continuous nature of the bremsstrahlung X-ray spectrum, obtaining quality bSPECT images requires an advanced reconstruction algorithm, including model-based attenuation, scatter, and collimator–detector response (CDR) compensations that are not yet widely established in the clinical settings. According to a study, PET imaging technology using ^{90}Y is more effective than bSPECT for evaluating the distribution of microspheres after radioembolization. While both SPECT and PET can detect hot spots larger than 10 mm, PET can identify smaller accumulations of activity that SPECT cannot. Furthermore, PET-based dose estimates using TOF technology are more precise than SPECT-based estimates, which tend to underestimate doses in high-dose regions. However, ^{90}Y PET requires a relatively long scan duration, which is 15 to 20 minutes per bed position. SPECT/CT reconstruction with a Monte Carlo–based system improved image contrast significantly and was in some cases higher (in larger hot spots) than PET/CT.[20]

To choose a post-treatment imaging modality, it is essential to note that there are systematic biases between different approaches regarding image acquisition and reconstruction algorithms, so interpreting and comparing dosimetric results between different groups should be done with caution.[9]

Post-treatment modality	Advantages	disadvantages
PET/CT	• Can identify smaller accumulations of activity • Higher spatial resolution • higher image contrast • PET-based dosimetry is more precise	• The relatively long scan duration • Not available everywhere
bSPECT/CT	• Widely available in daily clinical use • Less expensive than PET	• Needs advanced reconstruction algorithm

Table 3. Comparing PET/CT and bSPECT/CT for post-treatment imaging

Follow-up imaging

Following radioembolization, a clinical and biochemical evaluation is usually performed one to three months after treatment to assess the side effects. Imaging is usually performed three months post-radioembolization, followed by thrice-monthly imaging thereafter. The definition of "treatment response" and the best imaging method to evaluate this response may vary depending on the tumor's characteristics (e.g., FDG uptake) and the treatment goal.[19]

MRI

For over 20 years, MRI has been utilized for abdominal imaging and has undergone various technical advancements in sequence design and contrast media use, leading to improved diagnostic accuracy. These advancements have notably sharpened image quality and reduced motion and breathing-related artifacts.[21]

CT

CT has developed rapidly over the last decade. High spatial and temporal resolution imaging can be performed using scanners with 64 or more rows, allowing biphasic or triphasic liver examinations to be integrated with thoracic scans. Oncological therapy assessment has become incredibly efficient and accurate thanks to the fast acquisition times and high resolution of multidetector CT scanners. Although the imaging technique must be adapted to the underlying tumor entity, late-arterial-phase and portal-venous-phase abdominal CT are generally considered standard procedures.[22]

FDG-PET

FDG-PET can be an invaluable imaging modality after radioembolization mCRC. FDG-PET can also be employed in mCRC to monitor treatment progress and detect metastatic lesions that may not be visible with other imaging modalities. However, the effectiveness of FDG-PET in these cases may depend on several factors, including the stage of the disease, the timing relative to the radioembolization procedure, and the individual characteristics of the patient's cancer.[21]

Tumor response assessment and clinical outcome

Accurate assessment of the tumor is crucial for providing timely and effective treatment to patients with HCC. However, assessing the response to radioembolization for HCC is more complicated than doing the same for TACE or percutaneous ablation. There is no current consensus on the best time interval or criteria to use when evaluating the response to radioembolization. To comply with EASL-EORC[23] guidelines, a multiphasic MRI or CT should be performed one month after radioembolization and three months later. Traditionally, overall survival (OS) has been the primary measure of success in HCC treatment. However, with the emergence of more effective treatments for advanced HCC, alternative endpoints such as progression-free survival (PFS), tumor-free survival (TFS), time-to-progression (TTP), and objective response rate (ORR) have become increasingly important. These endpoints help researchers detect early signals of efficacy that can expedite regulatory approval. The assessment criteria for radioembolization are based on size assessment of representative tumors on MRI or CT. The Response Evaluation Criteria in Solid Tumors (RECIST) is the preferred assessment tool for solid tumors, evaluating complete or partial response (CR resp. PR) and stable disease (SD) or progressive disease (PD). Modified RECIST (mRECIST) criteria are proposed in the literature to evaluate tumor response for HCC.[24,25]

Adverse events

Radioembolization is generally a well-tolerated treatment but is not completely devoid of adverse events. Awareness of complications that may arise after the treatment and taking measures to prevent them is essential.[26]

Radioembolization-induced liver disease (REILD)

REILD is caused by microscopic occlusion of hepatic veins, hepatic congestion, and secondary necrosis of hepatocytes. The symptoms of REILD usually manifest four to eight weeks after radioembolization, including abnormal liver function, elevated bilirubin levels, and ascites, unless there are other causes, such as tumor progression or obstruction of the biliary duct.

Intrahepatic biliary dysfunction

A biliary adverse event is an uncommon complication that may arise after radioembolization, with reported rates ranging from 1.0% to 3.9%. This low incidence of complications is thought to be due to the microembolic effect of the microspheres used in radioembolization, which carry a lower risk of biliary necrosis than larger particles used in bland embolization and chemoembolization. Multicenter studies have shown that radioembolization does not significantly increase the risk of biliary injury in patients with cholangiocarcinoma or biliary obstruction. There is, however, a risk of parenchymal necrosis and a subsequent infection when ablative radioembolization (radiation segmentectomy) is utilized in patients with contaminated bile ducts. Some evidence suggests prophylactic antibiotics may reduce the risk of bilomas or hepatic abscesses, similar to their use in bland embolization and chemoembolization, although the effectiveness of these antibiotics in radioembolization has been questioned.

Local radiation to adjacent structures

According to theory, radiation from ^{90}Y can penetrate tissue at a mean depth of about 2.5 mm and a maximum of about 10 mm. No gastrointestinal ulceration was observed after radioembolization of left hepatic tumors within 1 cm of the stomach, according to a retrospective study assessing the effects of radioembolization. GI ulceration occurs more frequently following nontarget embolization than adjacent parenchymal radiation.[26]

1.3. Literature review

1.3.1. Heterogenous microspheres distribution following radioembolization

In radioembolization treatment, macroscopic hepatic vasculature information is necessary, but accurate dosimetry depends on the precise distribution of microspheres in hepatic microcirculation. The liver's small blood circulation starts when the left or right hepatic arteries split into even smaller arteries, with widths ranging from 50–100 micrometers. These small arteries then divide further into terminal arteries, with widths of 15–50 micrometers, eventually reaching the true capillary network, also called the sinusoids within the liver. This network has widths of just 5–10 micrometers and is a critical part of liver function. Meanwhile, the glass microspheres used are only 20–60 micrometers wide. Because the microspheres are so small, they are expected to get lodged evenly within the final small arteries of both normal and tumor tissue. However, even though many methods for calculating dose assume the microspheres are distributed uniformly in the liver, several studies have shown that the beads are deposited heterogeneously.

Fox et al. (1991) demonstrated significant heterogeneity in microsphere distribution following radioembolization treatment in a liver specimen. The authors analyzed two 1-cm^3 samples from different regions of a liver treated with resin microspheres, directly measuring the localized microsphere activity and absorbed doses. This study found that 86.2% of the tissue volume received less than the mean absorbed dose predicted by a uniform distribution model. Furthermore, up to 33.7% of the sample demonstrated absorbed doses less than one-third of the expected mean dose. Microscopic autoradiography revealed the clustering of microspheres around arterioles and capillaries rather than an even dispersal. Accordingly, this heterogeneous distribution was attributed to variations in local blood flow and streaming effects diverting microspheres.[27]

In a related study[28] the authors performed a histological examination on a 10 mm section of the resected liver treated with 6x107 resin microspheres (3.2 GBq).

In normal liver parenchyma, significant heterogeneity in microsphere distribution was noted, leading to large variances in absorbed dose. Within tumor tissue, microspheres preferentially clustered around the periphery rather than dispersing evenly. These peripheral clusters contained up to 65 microspheres in groups 20–1500 μm in diameter. Based on the microsphere localization data, dosimetric calculations revealed that the average absorbed dose exceeded 200 Gy within 6 mm of the tumor edge. The dose decreased sharply with increased distance from the tumor border. Due to peripheral

clustering, less than 1% of the normal liver tissue received an absorbed dose over 30 Gy. In larger tumors, the central portion received a minimal dose from the peripheral microspheres.[29]

Recent statistical analyses by Kao et al. [30] have further delineated the heterogeneity of resin microspheres within the liver. In one study, the authors examined over 250 tissue sections from a resected liver treated with radioembolization. Kao et al. found that the mean number of microspheres per section increased linearly with the cluster size, with aggregation occurring in small upstream arteries. This led to systematic heterogeneity, as clusters blocked flow to downstream arterioles. The authors' analysis showed that microsphere clustering induced significant structural nonuniformity in distribution.

In another study, Kao et al.[31] analyzed biopsies from a patient's normal liver parenchyma. They found that the coefficient of variation for activity concentration decreased as biopsy volume increased, indicating that heterogeneity in microsphere deposition is relevant at microscopic and macroscopic levels in the whole liver.

Together, these recent statistical studies provide extensive evidence that radioembolization microsphere distribution is inherently nonuniform because of preferential clustering. This is driven by hemodynamic factors causing aggregation within arterioles that impedes flow to downstream vessels. Accordingly, the study concluded that more spheres injected would cause greater dose inhomogeneity.

Given these studies, modified recommendations may arise regarding the current methodologies of clinical practice. Repeated radioembolization could become a standard practice to fully treat larger tumors. A higher threshold for administered doses based on current clinical dosimetric methods could be set. This higher threshold for administration may promote a more effective treatment due to a higher absorbed dose while minimally irradiating the normal hepatic parenchyma, which receives a fraction of the dose due to nonhomogenous microsphere distributions. [16, 27, 28, 313233]

Dosimetry implications arise when radiobiological and dosimetric effects would need to consider the heterogeneous microsphere deposition. Dosimetry would further be affected by the microanatomy of a patient's liver, cross-fire effects at the cellular level, microsphere bi-furcation effects within hepatic arteries, and the differences in therapeutic effect when different microsphere numbers and sizes are injected within a patient. Issues are explored elsewhere.[34, 35,36,37]

1.3.2. The importance of post-treatment imaging and dosimetry after ^{90}Y radioembolization

In 2012, Gates et al. showed that post-treatment ^{90}Y PET/CT imaging could be used as a standard practice after radioembolization to assess the localization of ^{90}Y glass microspheres in HCC patients.[38]

D'Arienzo demonstrated the correlation between an isodose map derived from ^{90}Y PET images in patients with liver metastasis treated with resin microspheres, which clearly indicated the accumulation of microspheres on the treated tumor site. This study also showed a strong correlation between the distribution of microspheres and the response of the tumor; the progression of metastasis was observed in an untreated area.[39]

In 2014, Lea et al. characterized the distribution of absorbed radiation dose after yttrium-90 glass microsphere radioembolization for hepatocellular carcinoma (HCC) using PET/CT. They analyzed 64 ^{90}Y PET/CT scans from patients with advanced HCC who underwent lobar treatments with intended target doses ranging from 83 to 129 Gy. Three-dimensional "dose maps" were created to visualize the radiation distribution in liver tumors and surrounding parenchyma. The study showed that recommended dosimetry and administration techniques resulted in high doses delivered to target tumors and background liver parenchyma, with moderate preferential uptake within tumors. However, there was significant variation in measured tumor and parenchymal doses, indicating the need to further develop patient-specific dosimetry techniques in hepatic radioembolization for HCC.[40]

A retrospective study investigated the radiation dose delivered to liver tumors and normal liver tissue using ^{90}Y microspheres in 56 patients with unresectable hepatocellular carcinoma (HCC). The distribution of microspheres within the liver was quantitatively assessed using post-treatment ^{90}Y PET/CT scans. The results showed that the tumors received a mean dose of 169 Gy. Tumor response by mRECIST criteria was performed for 48 tumors with follow-up scans. There were 21 responders (mean dose 215 Gy) and 27 non-responders (mean dose 167 Gy). The association between mean tumor absorbed dose and response suggests a trend but did not reach statistical significance ($p = 0.099$). The study highlights the importance of understanding the dose delivered to the tumor and normal liver tissue in predicting treatment outcomes and potential adverse events, providing valuable insights into the success or failure of radioembolization therapy for HCC.[41]

The study conducted by Kappadath in 2018 investigated the tumor dose-response characteristics of hepatocellular carcinoma (HCC) using voxel-level absorbed doses (D)

and biological effective doses (BED) based on quantitative ^{90}Y SPECT/CT after ^{90}Y radioembolization with glass microspheres. They analyzed 34 patients and segmented 53 tumors larger than 2.5 cm in diameter. Tumor response was evaluated using different criteria. The study found that tumor response (mRECIST) correlated significantly with D_{mean}, D_{20} to D_{80}, BED_{mean}, and BED_0 to BED_{80}. Threshold doses for a 50% probability of mRECIST response were 160 Gy for D_{mean} and 214 Gy for BED_{mean}. Tumor dose heterogeneity showed a significant correlation with tumor volume. Moreover, no complications were observed in patients with normal liver D_{mean} less than 44 Gy. The findings suggest that ^{90}Y radioembolization with glass microspheres at specific dose levels can predict tumor response with positive and negative predictive values of approximately 70% and 62%, respectively. Furthermore, normal liver D_{mean} below 44 Gy did not lead to complications in the patient cohort.[42]

In a retrospective study, 45 hepatocellular carcinoma (HCC) patients underwent ^{90}Y radioembolization using either glass or resin microspheres. After treatment, all patients underwent ^{90}Y PET/CT with time-of-flight reconstruction to assess dosimetric parameters. The tumor-absorbed dose and cumulative tumor dose-volume histogram were calculated using a dose point Kernel convolution algorithm. Radiological tumor response was evaluated using mRECIST criteria, and progression-free survival (PFS) and overall survival (OS) were analyzed. The study found that specific dosimetric thresholds correlated well with the radiological response, and a minimal absorbed dose of 40 Gy in 66% of the tumor volume (D_{66}) was highly predictive of tumor response, PFS, and OS, regardless of the type of microspheres used. The results suggest that dosimetric parameters obtained from ^{90}Y PET/CT can be valuable predictors of treatment response and patient outcomes. Hence, it is beneficial to implement systematic dosimetric evaluation in clinical practice to aid in predicting treatment efficacy and prognosis.[43]

1.4. The purpose of this study

The importance of ^{90}Y PET/CT imaging and dosimetry has been shown in several studies. However, despite the benefits associated with post-treatment imaging, implementing this workflow step is not a uniformly adopted practice. Currently, waiting for the follow-up image, which typically takes around three months, is the standard practice to assess the effectiveness of treatment and determine if retreatment is necessary. The rationale for this study is predicated on the need for an early and accurate review of the efficacy of ^{90}Y treatment. If found in this study that ^{90}Y PET/CT evaluation and dosimetry add clinical benefit for patients by identifying where there is an untreated tumor and potential sites of recurrence, then the inclusion of post-treatment PET/CT dosimetry is reasonable for these patients. This is significant as it would allow patients to be triaged at the earliest opportunity and put forward for retreatment, enabling resource savings and creating an expedited workflow for patients. Furthermore, there is no standardization of the dose metric used to predict treatment response in radioembolization patients. In current dosimetry methods, the average absorbed dose delivered to the tumor is one of the key dosimetry metrics to predict the tumor response. Previous literature recommended an average absorbed dose of 120 Gy for a complete response[44]. However, some patients demonstrate viable tumors on the follow-up despite receiving tumoricidal radiation doses exceeding the recommended dose. This study is designed to show tumor heterogeneity, resulting in sub-therapeutic dosing of portions of the tumor, which causes a heterogenous response within the tumor. By characterizing dose metrics within tumor sub-regions like isodose contours, this work aims to elucidate the relationship between local dose deposition and the area of necrosis on the follow-up image. If one of the isodose ranges gives a better match to the site of a necrosis tumor on the follow-up image, it indicates that the dose level corresponds to the biologically effective dose that induced the tumor radiation response.

2. Materials and methods

2.1. Study population

In this retrospective study of HCC* patients treated with glass microspheres, the following inclusion criteria were considered:

1. Tumor characteristics: The study focuses on patients with well-delineated tumors on the baseline image.
2. PET/CT image availability: Patients must have Positron Emission Tomography-Computed Tomography (PET/CT) imaging available immediately after the radioembolization treatment. This imaging helps assess the initial response to therapy, evaluate the microsphere distribution, and identify an untreated part of the tumor.
3. Available follow-up imaging: Patients must have follow-up imaging available following post-treatment. This follow-up is crucial for evaluating the tumor's response to the therapy and monitoring the sites of recurrence.
4. Patient's response to the treatment: Patients with a partial response were included. Patients with a complete response to the treatment and those with interval progression were excluded from the dataset.
5. Heterogeneous microsphere distribution or heterogeneous response to the treatment. **

* Patients with non-HCC metastasis were excluded because of the heterogeneity of tumor biology across multiple malignancies, especially given the small sample size.

** Heterogenous microspheres distribution on the ^{90}Y PET is recognized by the hot spot and cold spots within the tumor. Fig.4 Shows homogenous microsphere distribution after the treatment. This patient had a complete response to the treatment. These patients were excluded from the study population. However, patients with heterogenous microsphere distribution on the ^{90}Y PET or heterogenous response (partial response) (Fig.5) were included in this study.

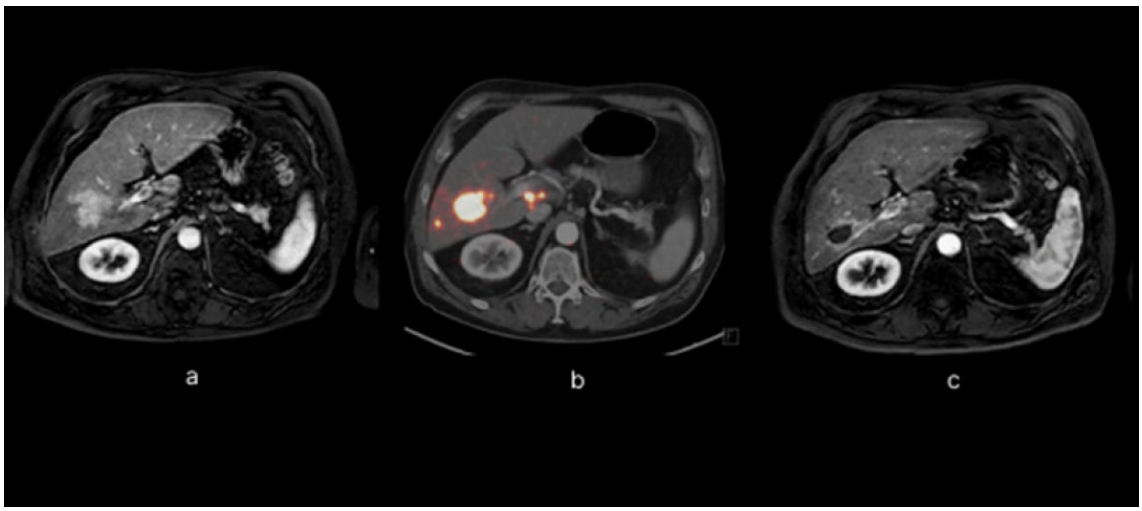

Fig. 4 Patient with HCC who received radioembolization with ^{90}Y glass microspheres. (a) The baseline image (MRI) demonstrated enhancing hepatocellular carcinoma in segment V/VI. (b) PET/CT image immediately after the treatment, ^{90}Y glass microspheres were selectively injected into the right hepatic artery. As shown, the microspheres are homogeneously distributed in the tumor located in segment V/VI. (c) Follow-up MRI 2 months after radioembolization showing complete response to the treatment as the tumor is no longer enhanced.

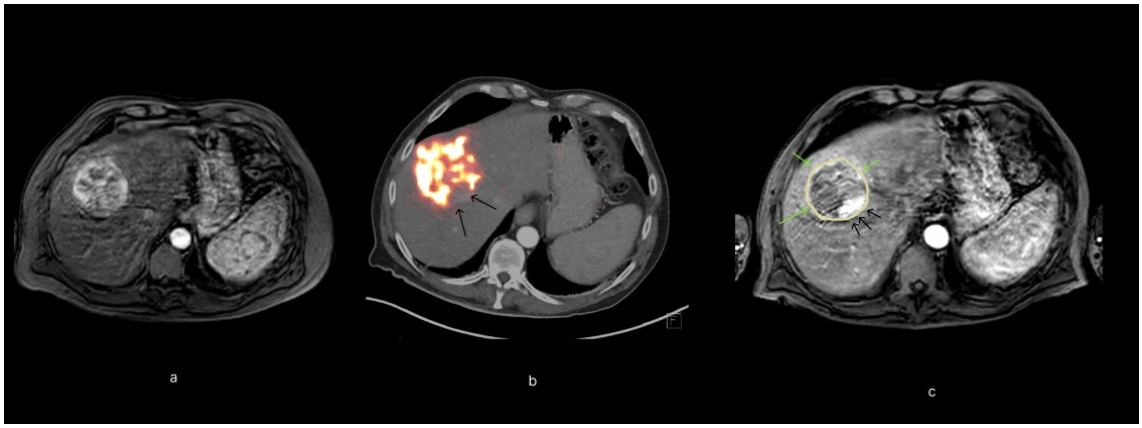

Fig. 5 Example of patient with heterogenous microsphere distribution and heterogenous response to the treatment. a) The baseline image (MRI) demonstrated hepatocellular carcinoma as an enhancement; b) On the PET/CT following treatment, black arrows show a part of the tumor that didn't receive microspheres; c) Tumor on MRI shows a heterogenous response to the treatment; this part uses green arrows to show how this part of the tumor responded to the treatment, meaning part of the tumor is dead (necrotic) while the other part of the tumor is still viable (black arrows).

2.2 ^{90}Y PET/CT

PET/CT data were acquired on a state-of-the-art Siemens mCT Time-Of-Flight (TOF) PET/CT scanner (Siemens Medical Solutions USA, Inc.). The mCT combines a whole-body LSO PET scanner with a 40-slice CT scanner. For maximum sensitivity, the PET component provides a wide acceptance angle of 13.2u and a 21.8 cm axial field-of-view (FOV). There is approximately a 43% overlap between consecutive bed positions in

whole-body mode. Jakoby et al.[45] performed a detailed characterization of the physical and clinical performance of the mCT.[45]

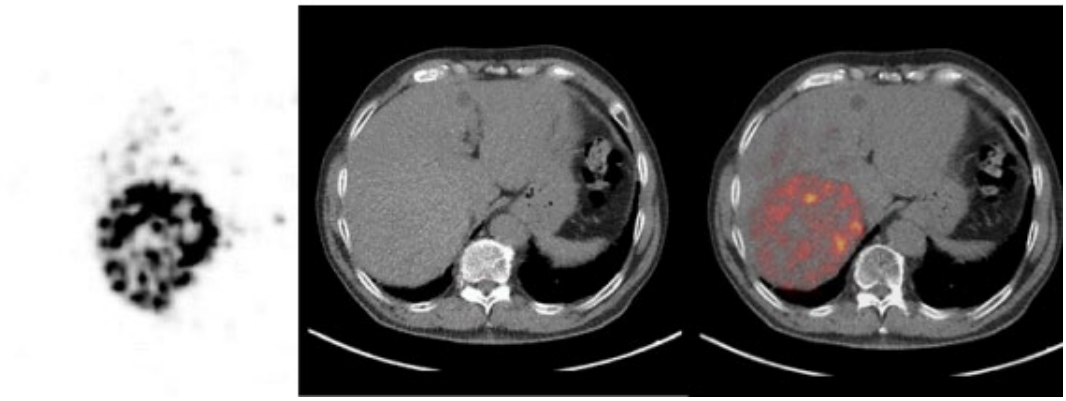

Fig. 6 Representative images of ^{90}Y PET/CT

2.3 The follow-up image

The follow-up image was acquired on CT or MRI.

2.4 Hepatic segmentation

Commercial dosimetry software, Simplicit90Y^{TM}, was used to create contours on PET/CT and the follow-up image. The tumor volumes were delineated on the CT acquired with the PET scan following ^{90}Y radioembolization. We preferably used the arterial phase for creating contours. Contours were individually drawn in the axial view of the CT. PET images were thresholded at 1% of maximum activity to determine the perfused volume of the injected liver. To calculate non-tumoral liver volume, total liver volume was subtracted from tumor volume. On the follow-up image, a nuclear physician contoured the viable tumor and necrosis. Subtracting the necrotic portion of the tumor from the whole tumor determined the viable tumor.

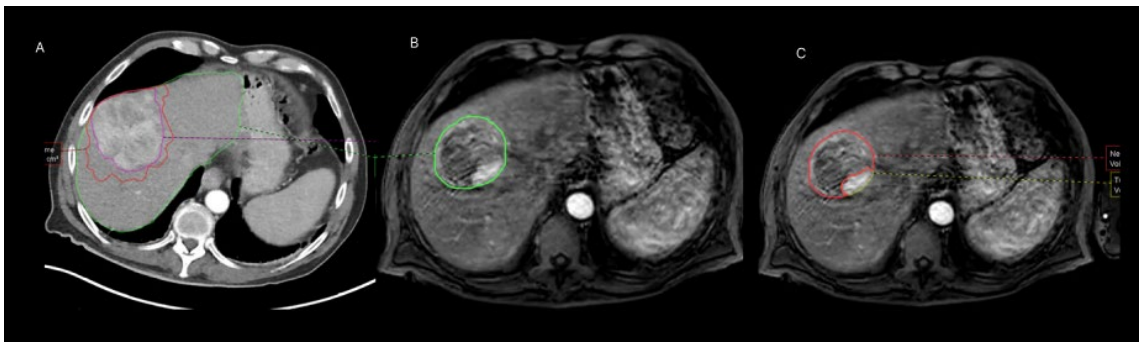

Fig. 7 Hepatic segmentation on PET/CT and the follow-up MRI: A) The green contour shows "whole liver," the red contour is "perfused volume," and the pink contour is "tumor"; B) MRI follow-up 3 months after 90Y radioembolization. The green contour shows the tumor appears on the follow-up MRI; C) The follow-up MRI: The red contour is "necrosis," which is part of the tumor that is dead at the time of the

follow-up; the yellow contour is a "viable tumor," meaning this part of the tumor is alive.In all cases, these volumes were saved as DICOM-RT structures and transposed on the ^{90}Y PET/CT studies.

2.5. Isodose contours

Commercial dosimetry software, MIM^{TM}, was used to create contours based on the isodose maps on the ^{90}Y PET image. Isodose contours from 100 to 400 Gy were created. (100, 120, 150, 180, 200 until 400 Gy). Isodose maps refer to the areas that receive the same dose within the tumor. In Fig.8, areas with the same colors refer to isodose maps.

The follow-up image was registered to the ^{90}Y PET/CT-derived isodose map, and the lesion contours were transferred. Using PET intensity as a guide, we manually fine-tuned the alignment if the automatic rigid registration wasn't satisfactory. This is the same process we use in our clinical dosimetry studies. A slight adjustment has been made to the PET to compensate for small inconsistencies in coregistration and volume variances between the 90Y PET and the follow-up image. The registration was performed once for each case and saved so that the contours of subsequent rounds could be imported without having to re-register the images.

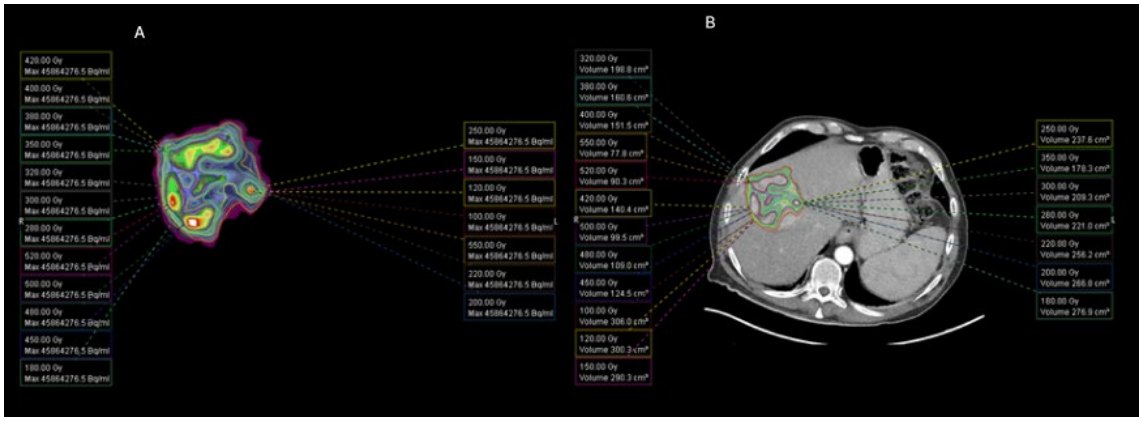

Fig. 8 A) Isodose maps illustrated on the PET image. Each color indicates the areas that received the same dose level. B) Isodose contours were transferred onto the anatomical image.

2.6. Image analysis

2.6.1. Quantitative assessment

To perform this comparison quantitatively, the Dice similarity coefficient will be used. The Dice coefficient is a similarity metric that measures the overlap between two contours. It is calculated by dividing the intersection of the contours twice by the sum of

their areas. A higher Dice coefficient indicates a better match between the contours. By utilizing the Dice coefficient, we comprehensively evaluate and compare the matching accuracy of each isodose contour with the viable tumor and necrosis contours outlined on the follow-up image. In this study, we assumed the tumor contour delineated on the follow-up image represents the ground truth tumor extent and radiation response. If an isodose contour touched the border of the viable tumor without extending into it, this contour level was interpreted as the average radiation dose received by the viable tumor, regardless of the mean absorbed dose by the whole tumor.

2.6.2. Qualitative assessment

In this study, qualitative assessment is also necessary in addition to quantitative assessment. The tumor's nature causes its morphology to change in response to treatment. Therefore, it is not always easy to compare the tumor's morphology before and after treatment using standard imaging assessment tools. For the qualitative assessment, a 1–5-point scale was established. A board-certified nuclear medicine physician then compared the viable tumor and/or necrosis on the follow-up image with the part of the tumor on the PET image that did not receive enough dose and/ or received a and rated the correlation visually.

5-point scale definition:

1: Very poor agreement: There is no correlation between the microsphere distribution on the post-treatment PET image and the site of necrosis and/or viable tumor on the follow-up image.

2: Poor agreement: This would mean that while there is some small correlation, it is not reliable enough to make predictions. It indicates a higher agreement than "very poor" but still suggests significant inconsistency between the PET and follow-up images regarding the site of necrosis and/or viable tumor.

3: Moderate agreement: This indicates a fair level of correlation between the two but is not strong enough to be reliable for retreatment planning based on the data from the PET image.

4: Good agreement: This implies a strong relationship between the microsphere distribution, necrosis, and/or viable tumor presence. Although this agreement is sufficient to predict the location of necrosis and/or viable tumors, the morphology of the activity distribution regions does not consistently align with the morphology of areas with necrosis and/or viable tumor.

5: Very good agreement: This implies a strong relationship between the microsphere distribution, necrosis, and/or viable tumor presence. The agreement is sufficient to

predict the location of necrosis and/or viable tumor; the morphology of the activity distribution regions consistently aligns with the morphology of areas with necrosis and/or viable tumor.

3. Result

Included patients in this study had heterogonous activity distribution due to the technical issues during microspheres administration or pathophysiology of the tumor. Patients have shown heterogeneous activity distribution on the post-treatment PET due to technical issues during the administration, including a selection of catheterization site and catheter position. This leads to missing an artery that targets the whole or part of the tumor (Fig. 9). And patients who have shown heterogeneous activity distribution on the PET image due to the pathophysiology of the tumor. The tumor often shows irregular blood supply, which leads to intra-tumoral preferential flow (Fig. 10). Altogether, 10 patients were included in this study. The median follow-up for these 10 patients was 91 days (range 46–125 days). The mean injected activity in the liver was 3.83 GBq. The average tumor absorbed dose based on ^{90}Y PET dosimetry for the patients was 264.2 Gy. The mean absorbed dose for the necrosis area contoured on the follow-up image was 488.3 Gy, and the mean absorbed dose for the viable tumor on the follow-up is 192.7 Gy. Table 4 illustrates the activity injected, D_{mean} of the tumor, the necrosis absorbed dose, and the viable tumor absorbed dose for all these patients.

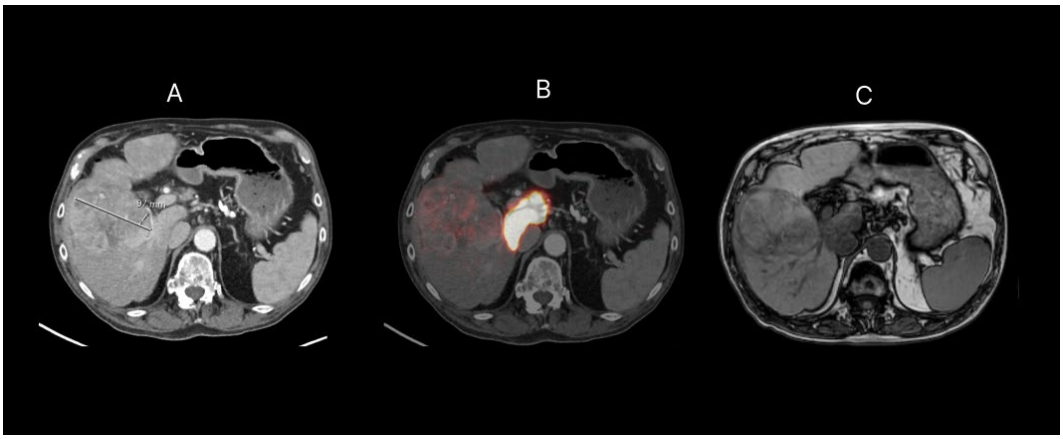

Fig. 9 A misplaced catheter during the radioembolization leads to activity accumulation outside the tumor. A) is a baseline image that shows the tumor size before treatment. B) Post-treatment PETCT shows the tumor received less than the planned dose due to the catheter being misplaced. C) The three-month follow-up image shows necrosis outside the tumor due to the treatment.

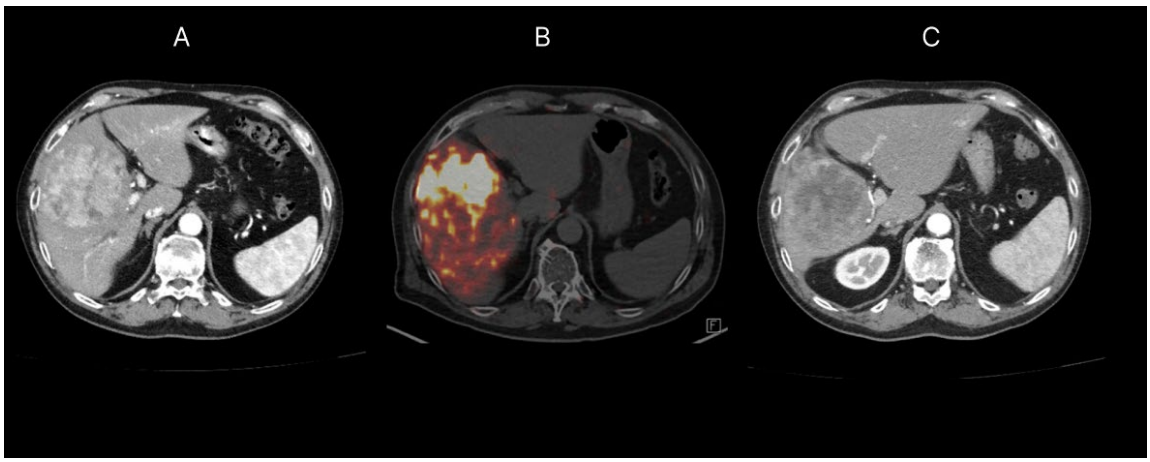

Fig. 10 Heterogenous activity distribution after the treatment due to the intra-tumoral preferential flow

	Injected Activity (GBq)	Average Absorbed Dose by Tumor (Gy)	Average Absorbed Dose by Necrosis (Gy)	Average Absorbed Dose by Viable Tumor (Gy)	Time interval between ^{90}YPET and the follow-up
Patient 1	2.80	384	302	256	90 days
Patient 2	4.40	461	559	199	104 days
Patient 3	6.60	267	519	263	85 days
Patient 4	2.02	93	184	53	125 days
Patient 5	0.97	181	312	105	91 days
Patient 6	11.33	309	479	369	46 days
Patient 7	0.80	390	555	304	114 days
Patient 8	7.06	271	971	202	91 days
Patient 9	1.16	197	327	28	79 days
Patient 10	1.22	189	675	148	96 days

Table 4. Representing injected activity, intra-tumoral dosimetry and time interval between ^{90}Y PET and the follow-up image.

Patient 2 intra-tumoral dosimetry is an example that illustrates the importance of intra-tumoral dosimetry. During the treatment, the tumor received an average absorbed dose of 461 Gy. However, there is still a viable tumor at the time of follow-up, which is not explainable by the mean absorbed dose that the tumor received during radioembolization. By further examining the activity distribution on post-treatment PET, it can be seen that heterogonous activity distribution results in a heterogonous absorbed dose inside the tumor. With intra-tumoral dosimetry, the yellow area of the tumor received a suboptimal dose of 199 Gy, which is significantly lower than the mean

absorbed dose. Creating isodose contours also reveals that the isodose range of 120 Gy–200 Gy touches the tumor border.

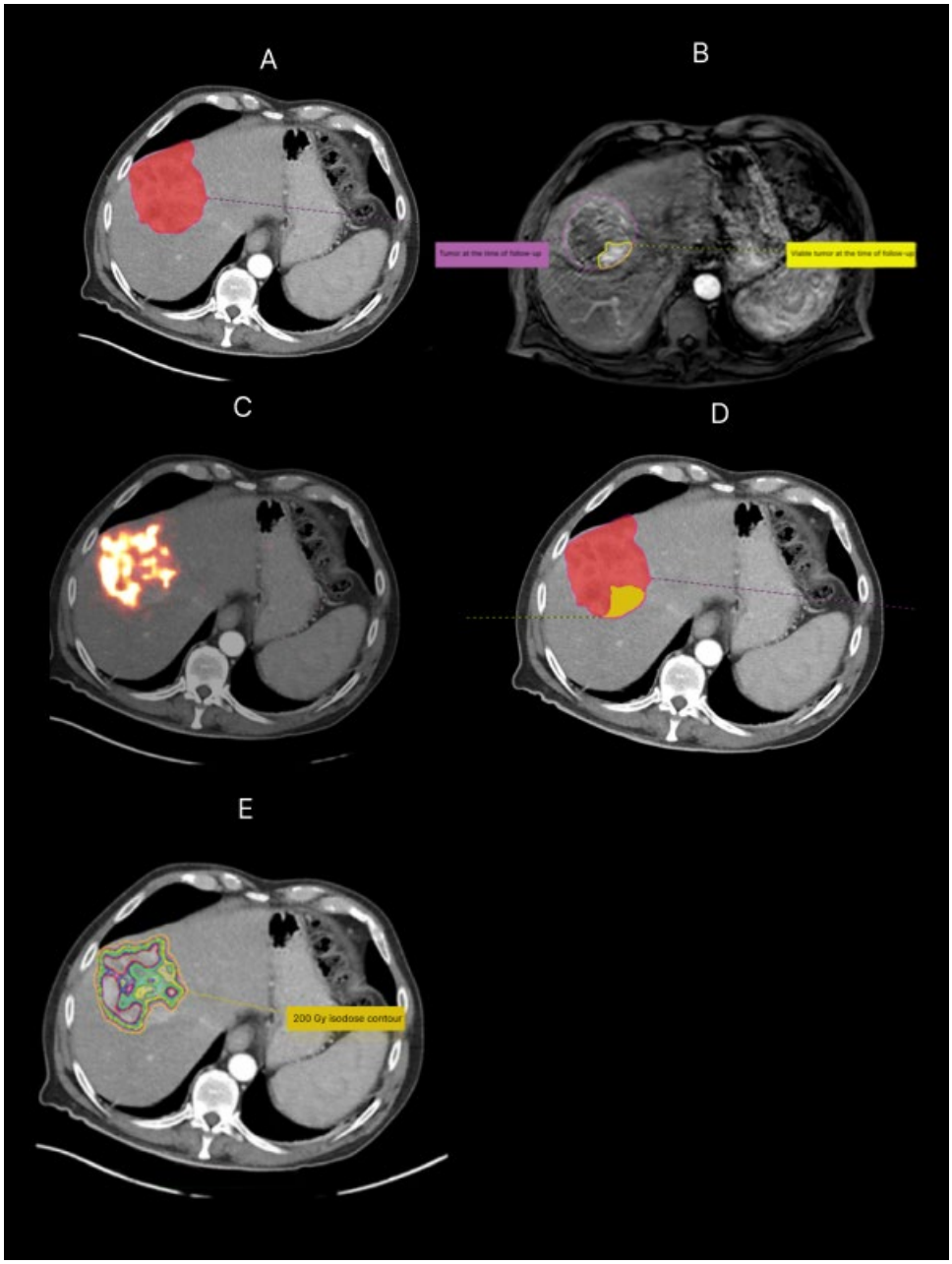

Fig. 11 The importance of intra-tumoral post-treatment PET/CT dosimetry. A) shows the tumor absorbed D_{mean} of 461 Gy during radioembolization. Nevertheless, a site of viable tumor still presents at the time of the follow-up (B). Post-treatment PET/CT (C) illustrates that the site of the tumor did not show the same level of accumulated activity as the other parts of the tumor. With intra-tumoral dosimetry (D, E), it has been shown that this part of the tumor received 120 Gy.

3.1. Quantitative assessment

The Dice coefficient was calculated at incremental isodose levels from 100 Gy up to 400 Gy, at 10 Gy intervals, for each of the 10 patients in the study. Particularly, this analysis generated 17 Dice coefficient data points per patient, assessing the spatial overlap between the PET-derived isodose contour and the contour of the necrotic region for each 10 Gy increment.

The Dice coefficient values showed variable levels of agreement between the PET isodose contours and the necrosis across patients. The maximum Dice coefficient for 10 patients ranged from 0.37 to 0.74 (mean 0.56), indicating the isodose contour that best matched the area of radiation necrosis. However, there was no single optimal isodose contour that perfectly aligned with the necrosis for all patients.

Further examination of the isodose levels associated with the peak Dice coefficients revealed a favorable range of 250–300 Gy. 8 out of 10 patients exhibited maximum Dice values for isodoses within this range. The remaining two patients had peak overlaps at 120 Gy and 480 Gy, respectively.

The Dice coefficient trends demonstrated a gradual increase across incremental isodose contours until reaching the maximum value, followed by a decline at higher doses. To precisely identify the ideal isodose, a ± 10 Gy range around the peak Dice contour was analyzed.

In summary, the incremental Dice coefficient analysis enabled quantitative identification of the PET-based isodose levels with the strongest spatial correspondence to radiation necrosis for this patient cohort. This indicates that the dose level corresponding to the peak Dice coefficient is likely the biologically effective dose that induced the tumor radiation response.

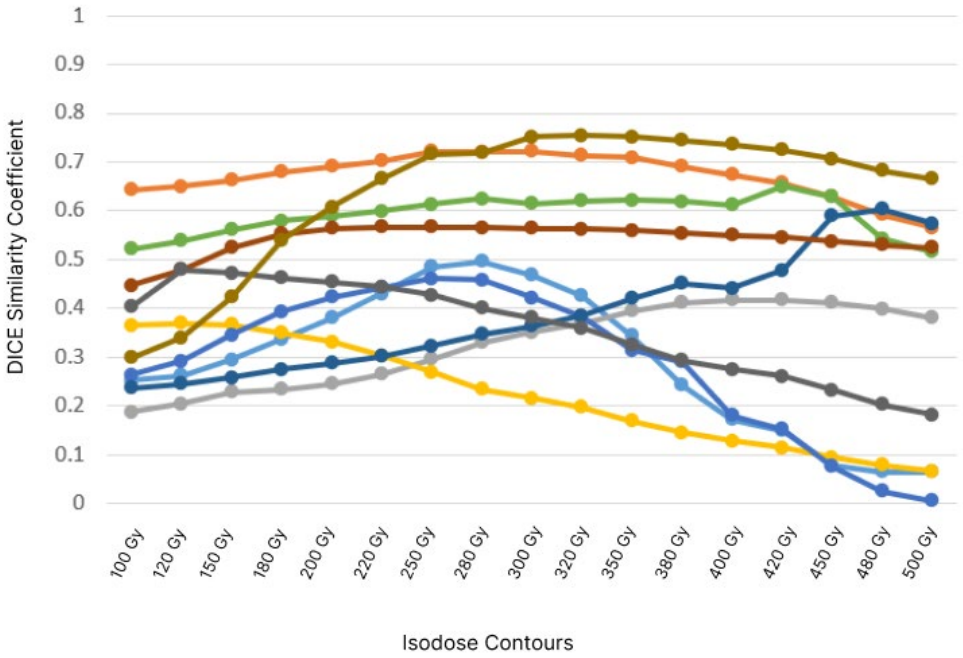

Fig. 12 Comparing DICE similarity coefficient for ten patients. For each patient, the dose level corresponding to the highest Dice coefficient is likely the biologically effective dose that induced the tumor radiation response.

3.2. Qualitative assessment

Qualitative assessment for 10 included patients shows a median agreement of 4 on a 5-point scale. 9 patients show a very good or good agreement activity distribution between ^{90}Y PET and the follow-up image, which means there is a strong relationship between the ^{90}Y microsphere distribution and necrosis and/or viable tumor on the follow-up image. 1 patient shows moderate agreement, which means that data acquired from ^{90}Y PET distribution is not reliable enough for treatment planning based on

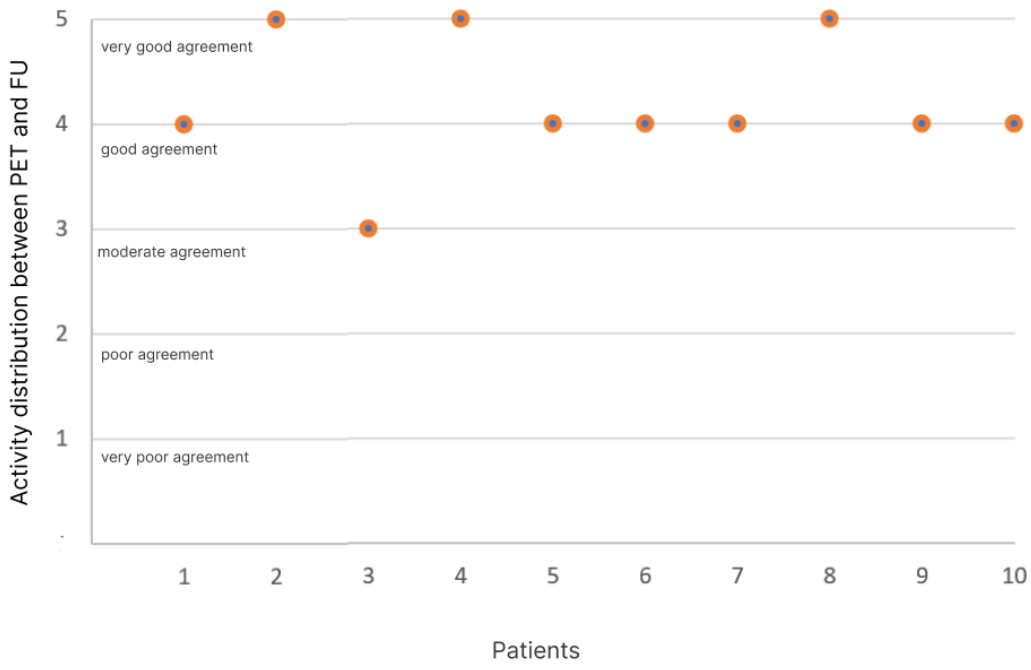

Fig.13. Qualitative assessment of activity distribution agreement between the post-treatment PET image and the site of necrosis and viable tumor on the follow-up image for 10 patients. Dr. Marnix Lam conducted the assessment.

4. Discussion

This retrospective study successfully demonstrated the importance of intra-tumoral post-treatment dosimetry in identifying the site of the viable tumor three months earlier than the follow-up image. In a clinical routine, the average absorbed dose (D_{mean}) is a key metric to predict the tumor response in ^{90}Y PET dosimetry after radioembolization. Sometimes in patients treated with radioembolization, it has been observed that despite the average absorbed dose being much higher than the recommended amount, there is still evidence of a viable tumor on the follow-up image. Conventional dosimetry methods cannot explain this. However, through intra-tumoral dosimetry, which is feasible with available dosimetry software, and creating isodose contours based on ^{90}Y dose distribution, we can predict the site of a viable tumor and necrosis within the tumor. Personalized intra-tumoral dosimetry is a step towards improving treatment planning, which can lead to a better clinical outcome. Based on the results of the quantitative assessment in this study for 10 patients, an isodose range of 250 Gy–300 Gy resulted in the most favorable concordance between the PET isodose contours and the site of necrosis on the follow-up.

In previously published data, the importance of ^{90}Y PET dosimetry in assessing the treatment response was shown. However, the focus of these studies is usually on the average absorbed dose within the tumor.[44,39,46,47] Unlike prior publications, this study concentrates on the importance of intra-tumoral dosimetry. Tumors are not uniform masses of cells but consist of a diverse population of cells with different genetic and phenotypic characteristics. This heterogeneity is crucial in response to the radioembolization treatment. Due to tumor heterogeneity, although the mean absorbed dose serves as a valuable metric for evaluating tumor response, its reliance alone is inadequate due to differential treatment responses exhibited by distinct tumor regions. Hence, the importance of intra-tumoral dosimetry in addressing tumor heterogeneity is to optimize treatment planning, predict response, and enhance therapeutic efficacy in radioembolization treatment.

Also, in clinical practice, the effectiveness of treatment is determined by assessing the tumor on the follow-up images. However, a significant challenge in assessing treatment response is the time interval between the treatment and follow-up images. On an early follow-up, persistent tumoral enhancement can be mistaken for a viable tumor and impact clinicians' decision-making. A recent study showed that pathologic complete response was not infrequent in cases that show a partial response according to EASL

criteria. This study showed the utility of ^{90}Y PET dosimetry in identifying a viable tumor. Hence, one potential solution to this challenge is to conduct a ^{90}Y PET.

This study has some limitations, particularly regarding quantitative assessment. The quantitative analysis of post-treatment PET/CT scans and subsequent follow-up images poses a unique challenge when significant tumor shrinkage is observed. It appears that the Dice score comparison between post-treatment PET/CT scans and follow-up images was not as high as expected due to the significant tumor shrinkage. When a tumor has shrunk substantially, the overlap between the post-treatment PET and the follow-up image will be small, resulting in a low Dice score. This may initially seem counterintuitive, as a low Dice score is usually interpreted as a lack of correlation between the high activity accumulated site on PET and the site of necrosis on the follow-up. Yet, in this case, a low Dice score may result from tumor shrinkage rather than an uncorrelated set.

Considering the above-mentioned issues with quantitative assessment, relying solely on the DICE score may not accurately capture the changes in contours before and after treatment. That's why qualitative assessment is more important for this study. Qualitative metrics have demonstrated a better outcome compared to quantitative metrics. Fig. 12 shows that the isodose map based on the PET image after the treatment and the orange contour, which is necrosis on the follow-up, almost have the same pattern. However, the dice between these two contours is 0.4, which doesn't represent a great match. However, this patient received a visual assessment score of 4 out of 5, indicating a significant correlation between the activity distribution and the necrotic area.

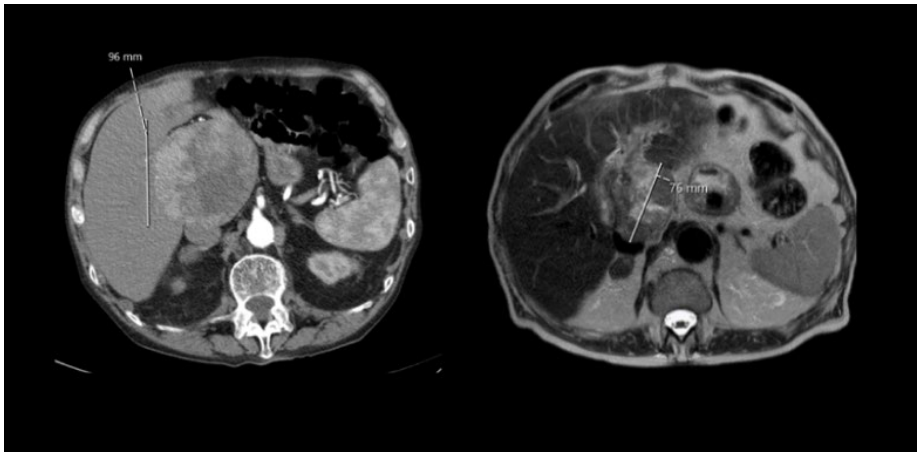

Fig. 14 Tumor shrinkage due to the treatment. The tumor diameter was 96 mm before radioembolization (on the left); and decreased to 76 mm after the treatment (on the right).

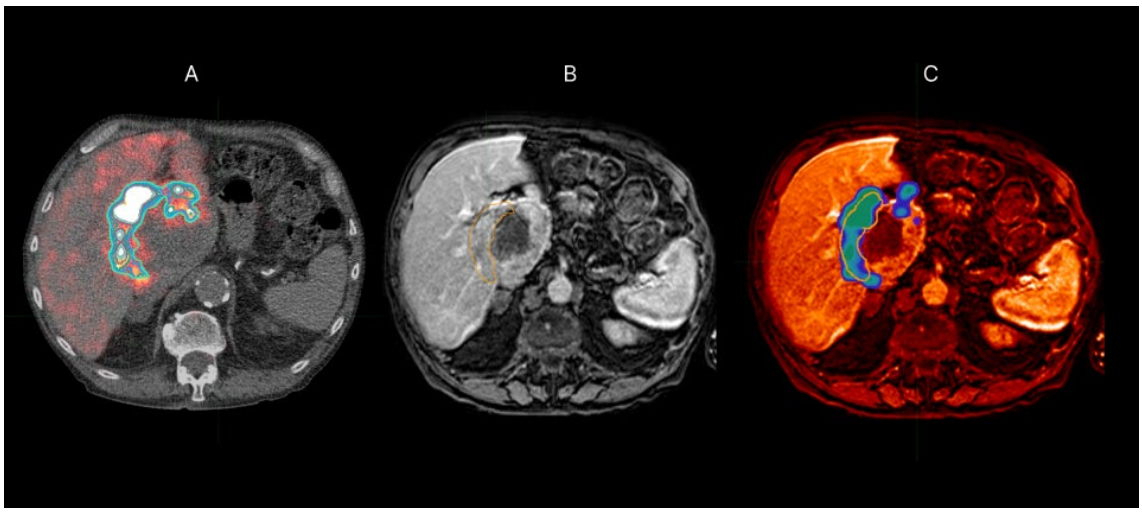

Fig. 15 Example of patients with a good overall agreement between the isodose contours on the PET/CT (A) and the necrosis contour on the follow-up image (B) The fusion of PET with the follow-up MRI (C) illustrates a similar pattern by visual assessment.

Another limitation of this study was the limited size of the dataset. Several factors were considered to ensure accurate patient selection for the project. Ideal patients would have tumors of appropriate size and shape, heterogeneous activity distribution on PET scans, and partial response to treatment. Though 130 HCC patients have undergone this treatment since 2015, only a limited number of them met the criteria for the assessment. In addition, gathering data at specific time intervals between PET/CT and the follow-up image would ideally provide more accurate data for this study. However, limitations in the available data hinder the ability to collect such comprehensive data sets.

Also, during the PET and the follow-up image registration, the precision and uncertainty of MR-PET image registration are mainly driven by the registration implementation and the quality of PET images due to their lower resolution and higher noise compared to the structural MR images. Uncertainty-aware visualization is crucial for image registration tasks where multiple images must be aligned to one point in space.

This study served as a proof of concept to highlight the importance of intra-tumoral dosimetry and qualitative and quantitative assessment between PET and follow-up imaging. While the study's findings provided initial insights, it is vital to acknowledge that a larger dataset is needed to confirm and validate these findings.

5. Conclusion

The wider availability of post-treatment ^{90}Y PET imaging should contribute to a better understanding of the distribution of microspheres used for the radioembolization of hepatic tumors. Regarding PET/CT after radioembolization, both qualitative and quantitative aspects should be considered together, as these two aspects are connected and each should be interpreted in the context of the other. With the isodose contours gained from ^{90}Y PET/CT, the intra-tumoral dosimetry of the PET/CT can be used as a tool for patient-specific dosimetry to improve treatment outcomes. Additional work to improve the quantitative nature of this intra-tumoral dosimetry method is needed. Nonetheless, the clearest message from our study appears to be that the contribution of ^{90}Y PET dosimetry is essential in assessing the treatment outcome.

6. Acknowledgments

I would like to express my gratitude to my mentor, Prof. Dr. Marnix Lam, and my supervisor, Clin. Sci. Grace Keane, for their unwavering support and encouragement in my professional development. Their willingness to provide guidance and answer my questions has been invaluable to my success. I strongly believe that my achievement today would not have been possible without the support I received from them. In addition, I would like to extend my thanks to Dr. Arthur Braat and Dr. Riku Klen for their clinical expertise and unending support.

7. References

1. Braat, A. J. A. T. *et al.* 90Y hepatic radioembolization: An update on current practice and recent developments. *Journal of Nuclear Medicine* **56**, 1079–1087 (2015).
2. Lin1', G. & Lunderquist1, A. *Portal Blood Supply of Liver Metastases Inga H#{228}gerstrand3*. www.ajronline.org (1984).
3. Lewandowski, R. J. & Salem, R. *Yttrium-90 Radioembolization of Hepatocellular Carcinoma and Metastatic Disease to the Liver*.
4. Biederman, D. M. *et al.* Outcomes of Radioembolization in the Treatment of Hepatocellular Carcinoma with Portal Vein Invasion: Resin versus Glass Microspheres. *Journal of Vascular and Interventional Radiology* **27**, 812-821.e2 (2016).
5. Vouche, M. *et al. Radiation lobectomy: Time-dependent analysis of future liver remnant volume in unresectable liver cancer as a bridge to resection*.
6. Lewandowski, R. J. *et al.* Radiation segmentectomy: Potential curative therapy for early hepatocellular carcinoma. *Radiology* **287**, 1050–1058 (2018).
7. Weber, M. *et al.* EANM procedure guideline for the treatment of liver cancer and liver metastases with intra-arterial radioactive compounds. *Eur J Nucl Med Mol Imaging* **49**, 1682–1699 (2022).
8. Louie, J. D. *et al.* Incorporating Cone-beam CT into the Treatment Planning for Yttrium-90 Radioembolization. *Journal of Vascular and Interventional Radiology* **20**, 606–613 (2009).
9. Bastiaannet, R. *et al.* The physics of radioembolization. *EJNMMI Physics* vol. 5 Preprint at https://doi.org/10.1186/s40658-018-0221-z (2018).
10. Keane, G., Lam, M. & De Jong, H. Beyond the MAA-Y90 Paradigm: The Evolution of Radioembolization Dosimetry Approaches and Scout Particles. *Semin Intervent Radiol* **38**, 542–553 (2021).
11. Wondergem, M. *et al.* 99mTc-macroaggregated albumin poorly predicts the intrahepatic distribution of 90Y resin microspheres in hepatic radioembolization. *Journal of Nuclear Medicine* **54**, 1294–1301 (2013).
12. Toskich, B. B. & Liu, D. M. Y90 Radioembolization Dosimetry: Concepts for the Interventional Radiologist. *Tech Vasc Interv Radiol* **22**, 100–111 (2019).
13. Sankhla, T. *et al.* Role of resin microsphere y90 dosimetry in predicting objective tumor response, survival and treatment related toxicity in surgically unresectable

colorectal liver metastasis: A retrospective single institution study. *Cancers (Basel)* **13**, (2021).

14. Bolch, W. E. *et al.* MIRD pamphlet No. 21: A generalized schema for radiopharmaceutical dosimetry-standardization of nomenclature. *Journal of Nuclear Medicine* **50**, 477–484 (2009).
15. Kennedy, A. S., Nutting, C., Coldwell, D., Gaiser, J. & Drachenberg, C. Pathologic response and microdosimetry of 90Y microspheres in man: Review of four explanted whole livers. *Int J Radiat Oncol Biol Phys* **60**, 1552–1563 (2004).
16. Giammarile, F. *et al.* EANM procedure guideline for the treatment of liver cancer and liver metastases with intra-arterial radioactive compounds. *Eur J Nucl Med Mol Imaging* **38**, 1393–1406 (2011).
17. Kim, S. P., Cohalan, C., Kopek, N. & Enger, S. A. A guide to 90Y radioembolization and its dosimetry. *Physica Medica* vol. 68 132–145 Preprint at https://doi.org/10.1016/j.ejmp.2019.09.236 (2019).
18. Lhommel, R. *et al.* Feasibility of 90Y TOF PET-based dosimetry in liver metastasis therapy using SIR-Spheres. *Eur J Nucl Med Mol Imaging* **37**, 1654–1662 (2010).
19. Levillain, H. *et al.* International recommendations for personalised selective internal radiation therapy of primary and metastatic liver diseases with yttrium-90 resin microspheres. doi:10.1007/s00259-020-05163-5/Published.
20. Elschot, M. *et al.* Quantitative Comparison of PET and Bremsstrahlung SPECT for Imaging the In Vivo Yttrium-90 Microsphere Distribution after Liver Radioembolization. *PLoS One* **8**, (2013).
21. Maas, M. *et al.* Follow-up after radiological intervention in oncology: ECIO-ESOI evidence and consensus-based recommendations for clinical practice. *Insights Imaging* **11**, (2020).
22. Kambadakone, A. R. & Sahani, D. V. Body Perfusion CT: Technique, Clinical Applications, and Advances. *Radiologic Clinics of North America* vol. 47 161–178 Preprint at https://doi.org/10.1016/j.rcl.2008.11.003 (2009).
23. Llovet, J. M. *et al.* EASL-EORTC Clinical Practice Guidelines: Management of hepatocellular carcinoma. *J Hepatol* **56**, 908–943 (2012).
24. Lencioni, R. & Llovet, J. M. Modified recist (mRECIST) assessment for hepatocellular carcinoma. *Seminars in Liver Disease* vol. 30 52–60 Preprint at https://doi.org/10.1055/s-0030-1247132 (2010).

25. Salem, R. & Thurston, K. G. Radioembolization with 90yttrium microspheres: A state-of-the-art brachytherapy treatment for primary and secondary liver malignancies - Part 1: Technical and methodologic considerations. *Journal of Vascular and Interventional Radiology* vol. 17 1251–1278 Preprint at https://doi.org/10.1097/01.RVI.0000233785.75257.9A (2006).
26. Laidlaw, G. L. & Johnson, G. E. Recognizing and Managing Adverse Events in Y-90 Radioembolization. *Seminars in Interventional Radiology* vol. 38 453–459 Preprint at https://doi.org/10.1055/s-0041-1735617 (2021).
27. Fox, R. A. *et al.* Dose distribution following selective internal radiation therapy. *Int J Radiat Oncol Biol Phys* **21**, 463–467 (1991).
28. Campbell, A. M., Bailey, I. H. & Burton, M. A. *Analysis of the distribution of intra-arterial microspheres in human liver following hepatic yttrium-90 microsphere therapy*. *Phys. Med. Biol* vol. 45 http://iopscience.iop.org/0031-9155/45/4/316 (2000).
29. Campbell, A. M., Bailey, I. H. & Burton, M. A. *Tumour dosimetry in human liver following hepatic yttrium-90 microsphere therapy INSTITUTE OF PHYSICS PUBLISHING PHYSICS IN MEDICINE Tumour dosimetry in human liver following hepatic yttrium-90 microsphere therapy*. *AND BIOLOGY Phys. Med. Biol* vol. 46 http://iopscience.iop.org/0031-9155/46/2/315 (2001).
30. Högberg, J. *et al.* Heterogeneity of microsphere distribution in resected liver and tumour tissue following selective intrahepatic radiotherapy. *Psychon Bull Rev* **4**, (1997).
31. Högberg, J. *et al.* Increased absorbed liver dose in Selective Internal Radiation Therapy (SIRT) correlates with increased sphere-cluster frequency and absorbed dose inhomogeneity. *EJNMMI Phys* **2**, 1–17 (2015).
32. Lam, M. G. E. H. & Smits, M. L. J. Value of 99mTc-macroaggregated albumin SPECT for radioembolization treatment planning. *Journal of Nuclear Medicine* vol. 54 1681–1682 Preprint at https://doi.org/10.2967/jnumed.113.123281 (2013).
33. Lewandowski, R. J. *et al.* Sustained safety and efficacy of extended-shelf-life 90Y glass microspheres: Long-term follow-up in a 134-patient cohort. *Eur J Nucl Med Mol Imaging* **41**, 486–493 (2014).
34. Walrand, S., Hesse, M., Jamar, F. & Lhommel, R. A hepatic dose-toxicity model opening the way toward individualized radioembolization planning. *Journal of Nuclear Medicine* **55**, 1317–1322 (2014).

35. Walrand, S., Hesse, M., Chiesa, C., Lhommel, R. & Jamar, F. The low hepatic toxicity per gray of 90Y glass microspheres is linked to their transport in the arterial tree favoring a nonuniform trapping as observed in posttherapy PET imaging. *Journal of Nuclear Medicine* **55**, 135–140 (2014).
36. Gulec, S. A., Sztejnberg, M. L., Siegel, J. A., Jevremovic, T. & Stabin, M. Hepatic structural dosimetry in 90Y microsphere treatment: A Monte Carlo modeling approach based on lobular microanatomy. *Journal of Nuclear Medicine* **51**, 301–310 (2010).
37. Pasciak, A. S., Bourgeois, A. C. & Bradley, Y. C. A microdosimetric analysis of absorbed dose to tumor as a function of number of microspheres per unit volume in 90Y Radioembolization. *Journal of Nuclear Medicine* **57**, 1020–1026 (2016).
38. Gates, V. L., Esmail, A. A. H., Marshall, K., Spies, S. & Salem, R. Internal pair production of 90Y permits hepatic localization of microspheres using routine PET: proof of concept. *Journal of Nuclear Medicine* **52**, 72–76 (2011).
39. D'Arienzo, M. *et al.* 90Y PET-based dosimetry after selective internal radiotherapy treatments. *Nucl Med Commun* **33**, 633–640 (2012).
40. Lea, W. B. *et al.* Microsphere localization and dose quantification using positron emission tomography/CT following hepatic intraarterial radioembolization with yttrium-90 in patients with advanced hepatocellular carcinoma. *Journal of Vascular and Interventional Radiology* **25**, 1595–1603 (2014).
41. Srinivas, S. M. *et al.* Determination of radiation absorbed dose to primary liver tumors and normal liver tissue using post radioembolization 90Y PET. *Front Oncol* **4**, (2014).
42. Kappadath, S. C. *et al.* Hepatocellular Carcinoma Tumor Dose Response After 90Y-radioembolization With Glass Microspheres Using 90Y-SPECT/CT-Based Voxel Dosimetry. *Int J Radiat Oncol Biol Phys* **102**, 451–461 (2018).
43. d'Abadie, P. *et al.* Prediction of tumor response and patient outcome after radioembolization of hepatocellular carcinoma using 90Y-PET-computed tomography dosimetry. *Nucl Med Commun* 747–754 (2021) doi:10.1097/MNM.0000000000001395.
44. Strigari, L. *et al.* Efficacy and toxicity related to treatment of hepatocellular carcinoma with 90Y-SIR spheres: Radiobiologic considerations. *Journal of Nuclear Medicine* **51**, 1377–1385 (2010).
45. Jakoby, B. W. *et al.* Physical and clinical performance of the mCT time-of-flight PET/CT scanner. *Phys Med Biol* **56**, 2375–2389 (2011).

46. Bourgeois, A. C., Chang, T. T., Bradley, Y. C., Acuff, S. N. & Pasciak, A. S. Intraprocedural yttrium-90 positron emission tomography/CT for treatment optimization of yttrium-90 radioembolization. *Journal of Vascular and Interventional Radiology* **25**, 271–275 (2014).
47. Chang, T. T., Bourgeois, A. C., Balius, A. M. & Pasciak, A. S. Treatment modification of yttrium-90 radioembolization based on quantitative positron emission tomography/CT imaging. *Journal of Vascular and Interventional Radiology* **24**, 333–337 (2013).